Exchange interactions and intermolecular hybridization in a spin-1/2 nanographene dimer

N. Krane[1*], E. Turco[1*], A. Bernhardt[2*], D. Jacob[3,4*], G. Gandus[5], D. Passerone[1], M. Luisier[5], M. Juríček[2#], R. Fasel[1,7], J. Fernández-Rossier[6#], and P. Ruffieux[1#]

[1] *nanotech@surfaces Laboratory, Empa - Swiss Federal Laboratories for Materials Science and Technology, Dübendorf, Switzerland*

[2] *Department of Chemistry, University of Zurich, Zurich, Switzerland*

[3] *Departamento de Polímeros y Materiales Avanzados: Física, Química y Tecnología, Universidad del País Vasco UPV/EHU, Av. Tolosa 72, E-20018 San Sebastián, Spain*

[4] *IKERBASQUE, Basque Foundation for Science, Plaza Euskadi 5, E-48009 Bilbao, Spain*

[5] *Integrated Systems Laboratory, ETH Zürich, Switzerland*

[6] *International Iberian Nanotechnology Laboratory (INL), 4715-330 Braga, Portugal*

[7] *Department of Chemistry, Biochemistry and Pharmaceutical Sciences, University of Bern, 3012 Bern, Switzerland*

*These authors contributed equally to this work.

#Corresponding authors:
michal.juricek@chem.uzh.ch
joaquin.fernandez-rossier@inl.int
pascal.ruffieux@empa.ch

Phenalenyl is a radical nanographene with triangular shape that hosts an unpaired electron with spin *S* = ½. The open-shell nature of phenalenyl is expected to be retained in covalently bonded networks. Here, we study a first step in that direction and report the synthesis of the phenalenyl dimer by combining in-solution synthesis and on-surface activation and its characterization both on Au(111) and on a monolayer of NaCl on top of Au(111) by means of inelastic electron tunneling spectroscopy (IETS). IETS shows inelastic steps that, together with a thorough theoretical analysis, are identified as the singlet–triplet excitation arising from interphenalenyl exchange. Two prominent features of our data permit to shed light on the nature of spin interactions in this system. First, the excitation energies with and without the NaCl decoupling layer are 48 and 41 meV, respectively, indicating a significant

renormalization of the spin excitation energies due to exchange with the Au(111) electrons. Second, a position-dependent bias-asymmetry of the height of the inelastic steps is accounted for by an interphenalenyl hybridization of the singly occupied phenalenyl orbitals that is only possible via third neighbor hopping. This hybridization is also essential to activate kinetic interphenalenyl exchange. Our results set the stage for future work on the bottom-up synthesis of spin *S* = ½ spin lattices with large exchange interaction.

Phenalenyl is a polycyclic conjugated hydrocarbon that possesses a magnetic ground state with spin *S* = ½, whereby an unpaired electron is hosted in a non-bonding π-molecular orbital. Its experimental study has been hampered by its high chemical reactivity, typical of radical species[1]. Recent progress in the on-surface synthesis and manipulation under ultra-high vacuum conditions has now made it possible to overcome this problem and study the electronic properties of unsubstituted phenalenyl on a gold surface[2]. Inelastic electron tunneling spectroscopy (IETS)[3] based on scanning tunneling microscopy (STM) shows a prominent zero bias peak that is associated with the formation of a Kondo singlet between the unpaired electron of the phenalenyl and the conduction electron of the surface, endorsing the picture of phenalenyl as a *S* = ½ molecule.

Two possible applications can be foreseen for this type of molecules. First, as in the case of the larger *S* = 1 triangulene[4–9] and other open-shell nanographenes[10–14], phenalenyl could serve as a building block for covalent nanographene arrays that behave as chains or lattices of *S* = ½ interacting spins[15]. Both the low spin and the small magnetic anisotropy make these artificial spin networks suitable to explore quantum magnetism, and perhaps to be used for engineering electronic phases with topological order that can be used for robust quantum information processing. Second, *S* = ½ objects provide a natural realization of spin qubits.

Progress in these two directions requires the understanding, and eventually the control, of exchange interactions of phenalenyl, both with the substrate and with other molecules when integrated within covalent arrays. Here, we undertake the first steps in this direction, both by exploring the electronic properties of a phenalenyl dimer (hereafter referred to as diphenalenyl) on a conducting surface as well as by including a decoupling layer between diphenalenyl and the conducting substrate.

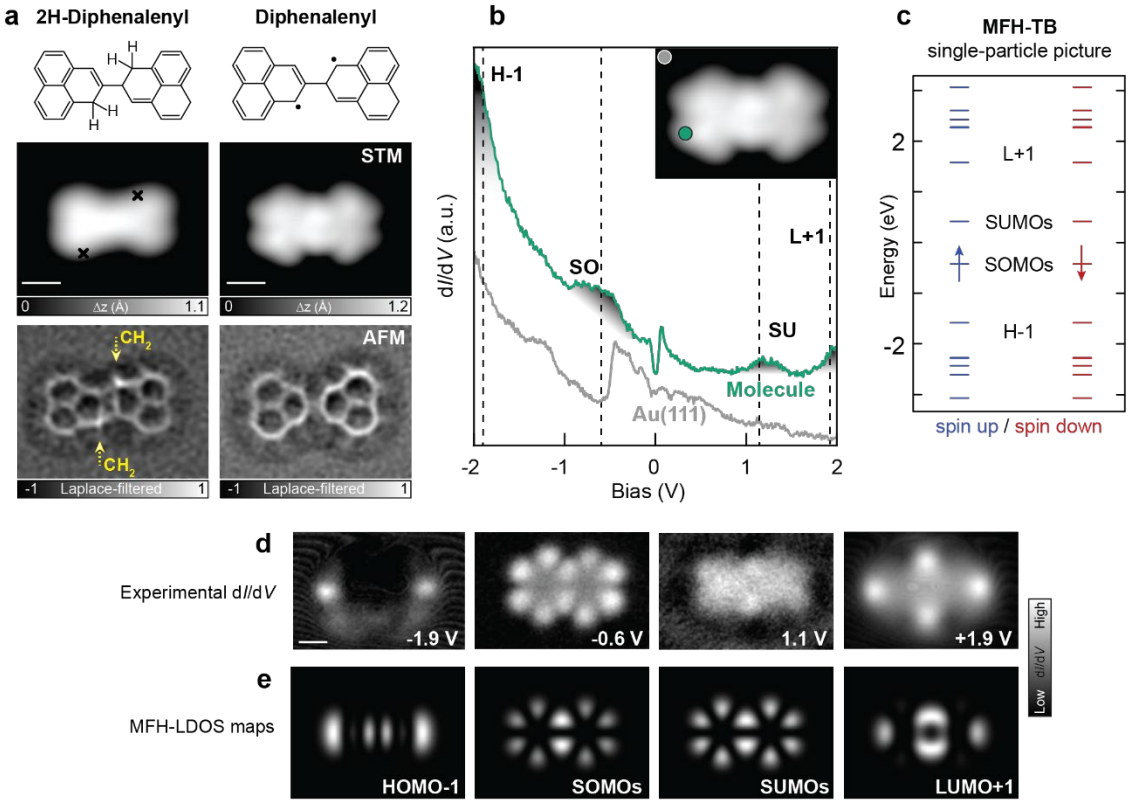

Figure 1. (a) Tip-induced activation of diphenalenyl on Au(111). STM (top) and nc-AFM (bottom) images before and after dehydrogenation via voltage pulses (black crosses). The images were taken with CO tip at closed feedback with -100 mV/50 pA (STM) and opened feedback on Au(111) with -5 mV/100 pA, Δ*z* = 1.8 Å (AFM). (**b**) dI/dV spectroscopy taken with CO tip on diphenalenyl (green) and Au(111) (grey), revealing the SOMOs and SUMOs at -0.6 V and +1.1 V, respectively, as well as the onsets of the HOMO-1 and LUMO+1 at -1.9 V and +1.9 V. The inset displays the positions, where the spectra were taken. Feedback loop opened at -2 V/350 pA, V_{rms} = 20 mV. Dashed lines mark energies of dI/dV maps displayed in (d). (**c**) MFH Energy diagram of the single-particle states. (**d,e**) Constant current dI/dV maps and MFH calculated projected density of states of the corresponding orbitals. HOMO-1 and LUMO+1 taken at 250 pA and V_{rms} = 30 mV, SOMOs and SUMOs at 200 pA and V_{rms} = 14 mV. Scale bars: 0.5 nm (a, d).

The preparation of diphenalenyl is achieved through a combined solution and on-surface synthesis approach. In the solution phase, the 2*H*-diphenalenyl precursor is synthesized in a sequence of nine steps starting from naphthalene (for details, see the SI). The use of hydro precursors has the advantage that activation of the target open-shell compound can be achieved using atom manipulation with a scanning tunneling microscopy (STM) tip[8] and does not necessarily require the catalytic action of metal substrates. We have recently shown that phenalenyl and triangulene can be achieved through selective activation of the corresponding hydro precursors using controlled voltage pulses from the STM tip[2]. Here, we follow a similar

approach to sequentially activate the two hydro-phenalenyl subunits of the precursor. The substrate was prepared by sublimation of NaCl on a clean Au(111) surface held at room temperature, which leads to a sub-monolayer coverage of NaCl organized into 1ML and 2ML islands. The molecular 2*H*-diphenalenyl precursor was deposited by sublimation onto the previously prepared sample, kept at a temperature of about 100 K during the deposition and rapidly transferred into the STM. An overview STM image of the so-obtained sample is reported in Figure S2, where, the molecular precursors can be found in sub-monolayer coverage adsorbed both on the Au(111) surface and NaCl islands. Sequential tip-induced cleaving of the hydrogen atoms from the sp^3 carbon atoms[2,8] yields the target diphenalenyl diradical, as proven by constant-height nc-AFM measurements of the precursor and the target compound (Figure 1a, bottom) both adsorbed on Au(111). The precursor molecules adsorbed on 1ML NaCl were similarly manipulated into diphenalenyl diradical as shown in Figure S2 (b,c). The change in the electronic structure can also be observed in the STM images (Figure 1a), showing distinct lobes and nodal planes for the activated molecule. Constant-height d*I*/d*V* spectroscopy of the activated molecule adsorbed on Au(111) is shown in Figure 1b, revealing the presence of two distinct resonances at –0.6 eV and 1.1 eV, and the onset of two conductance peaks at ±1.9 eV. To do a first assignment of the observed conductance peaks to the respective molecular orbitals, we used a tight-binding (TB) level of theory, taking into account the electron–electron Coulomb repulsion within the mean-field Hubbard (MFH) approximation. The calculated energy diagram reported in Figure 1c features two frontier states, commonly denoted as singly occupied and unoccupied molecular orbitals, SOMOs and SUMOs, respectively[16]. A comparison of the calculated local density of states (LDOS) and the experimental d*I*/d*V* maps of the molecule's electronic resonances allows a clear assignment of the experimentally observed resonances (Figure 1d,e).

In order to probe the magnetic properties of diphenalenyl, d*I*/d*V* spectroscopy at low bias voltages was conducted both on Au(111) and monolayer NaCl. As displayed in Figure 2a, the spectra show steps in the differential conductance at ± 41 mV and ±48 mV for the molecules on Au(111) and NaCl, respectively. Ovchinnikov's rule[17] and Lieb's theorem[18] predict the single spins of the two phenalenyl units to form an $S = 0$ ground state. For two coupled spins with $S = ½$ and Heisenberg coupling $J\boldsymbol{S_1}\cdot\boldsymbol{S_2}$, the excited state is $S = 1$ with energy $E = J$.

Therefore, the observed steps in differential conductance can be assigned to spin excitations from the singlet ground state to the triplet excited state.

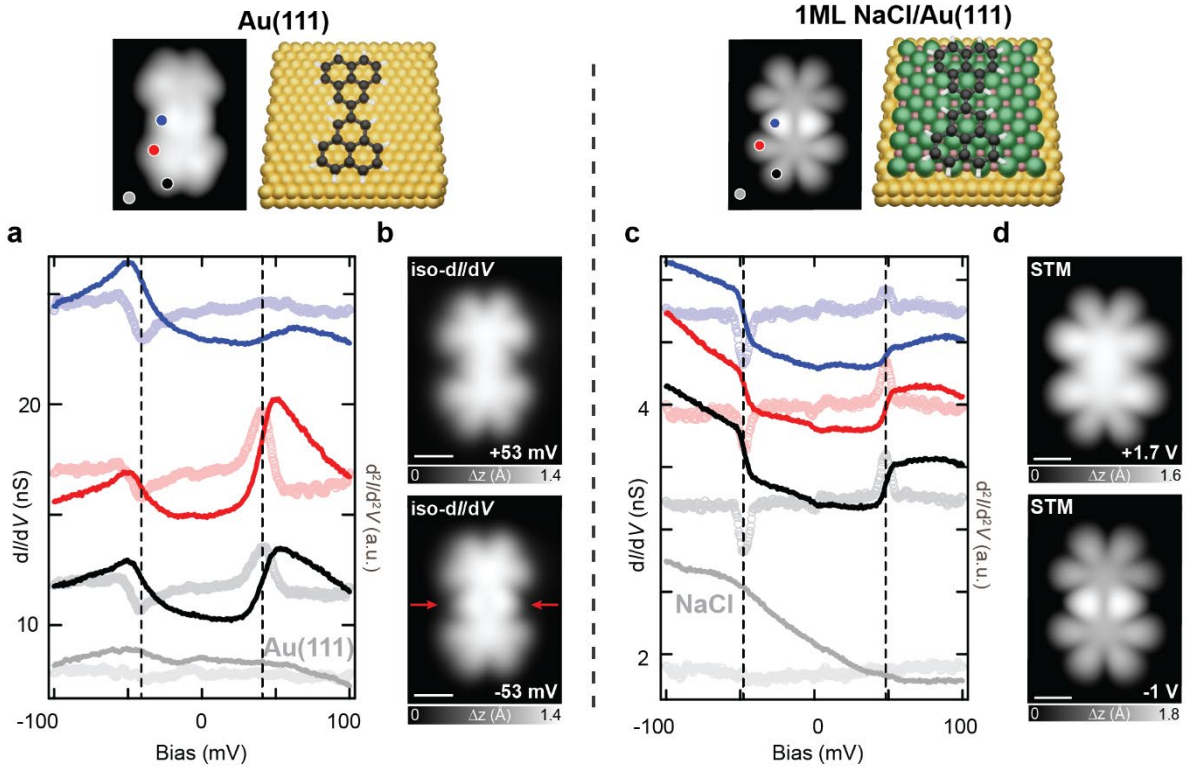

Figure 2. Inelastic spectroscopy of the spin excitations of diphenalenyl on Au(111) and 1ML-NaCl/Au(111). (**a**) d*I*/d*V* spectroscopy (solid lines) and second derivative (circles) of diphenalenyl adsorbed on Au(111). Tip positions are marked in the image above and the reference spectrum (bottom) is taken on Au(111). The dotted vertical lines mark the dip/peak positions of the second derivative at ±41 mV. Feedback opened at -100 mV/750 pA; V_{rms} = 2 mV (**b**) Constant d*I*/d*V* images (10 nS, V_{rms} = 3.5 mV) taken at energies above spin excitation. The red arrows in bottom panel highlight the asymmetry for different bias polarities. (**c**) d*I*/d*V* spectroscopy (solid lines) and second derivative (circles) of diphenalenyl on monolayer NaCl. Tip positions are marked in the image above and the reference spectrum (bottom) is taken on NaCl. Dotted vertical lines at dip/peak of second derivative at ±48 mV. Feedback opened at -100 mV/250 pA; V_{rms} = 2.8 mV (**d**) Constant current STM images (20 pA) of diphenalenyl on NaCl/Au(111) taken at the onset energies of the frontier orbitals, displaying the asymmetry of the SOMOs and SUMOs. Scale bars: 0.5 nm (b, d).

A specific feature of our system is the marked asymmetry of the height of the conductance steps in Figure 2a. The d*I*/d*V* spectra taken between the phenalenyl units (blue lines) show a higher step at negative bias polarity, compared to the smaller step at positive bias polarity. This effect can be seen for diphenalenyl on Au(111) as well as on NaCl islands. Figure 2b displays two iso-d*I*/d*V* maps[19], using the d*I*/d*V* signal as feedback, taken at energies just outside of the spin excitation gap. The asymmetry with bias polarity becomes clearly visible. Therefore, the asymmetry of the spectra taken in the center of the dimer is an intrinsic property of the diphenalenyl molecules and independent from the underlying substrate. On the other hand, for the molecule deposited on Au(111), the inelastic steps are broadened and show pronounced triangular overshoots. For the spectra taken at the sides of the molecule these overshoots are significantly larger for positive bias (Figure 2a). This asymmetry is not present when the molecule is adsorbed on NaCl, and thus is non-generic. As discussed below, our calculations are able to account for both asymmetries.

Importantly, there are three main differences between the spectra acquired for diphenalenyl on Au(111) with those taken on NaCl. First, the singlet–triplet excitation energy is significantly higher on NaCl with 48 meV, compared to 41 meV on Au(111). Second, the peak-like features at the excitation steps are not present in the spectra taken on NaCl and, third, the width of the steps is much broader on Au(111) than on NaCl. The latter becomes apparent in the numerical derivation of the d*I*/d*V* signal in Figure 2a.

We now resort to theory to rationalize the main properties of the observed inelastic excitations by addressing i) their different energies and broadening, depending on the presence, or not, of a NaCl decoupling layer, and ii) the bias asymmetry of the excitation line shapes. First, we provide evidence that inelastic excitations observed at around 40 meV are associated with interphenalenyl exchange. For that matter, following our previous works,[4,20,21,] we build a generalized Hubbard model, that also includes long-range Coulomb interactions (see SI for computational methods). Our calculations show that diphenalenyl remains open-shell, possessing an $S = 0$ ground state and an $S = 1$ excited state with energy in

the range of the experimental observations. Thus, diphenalenyl hosts two antiferromagnetically coupled unpaired spins.

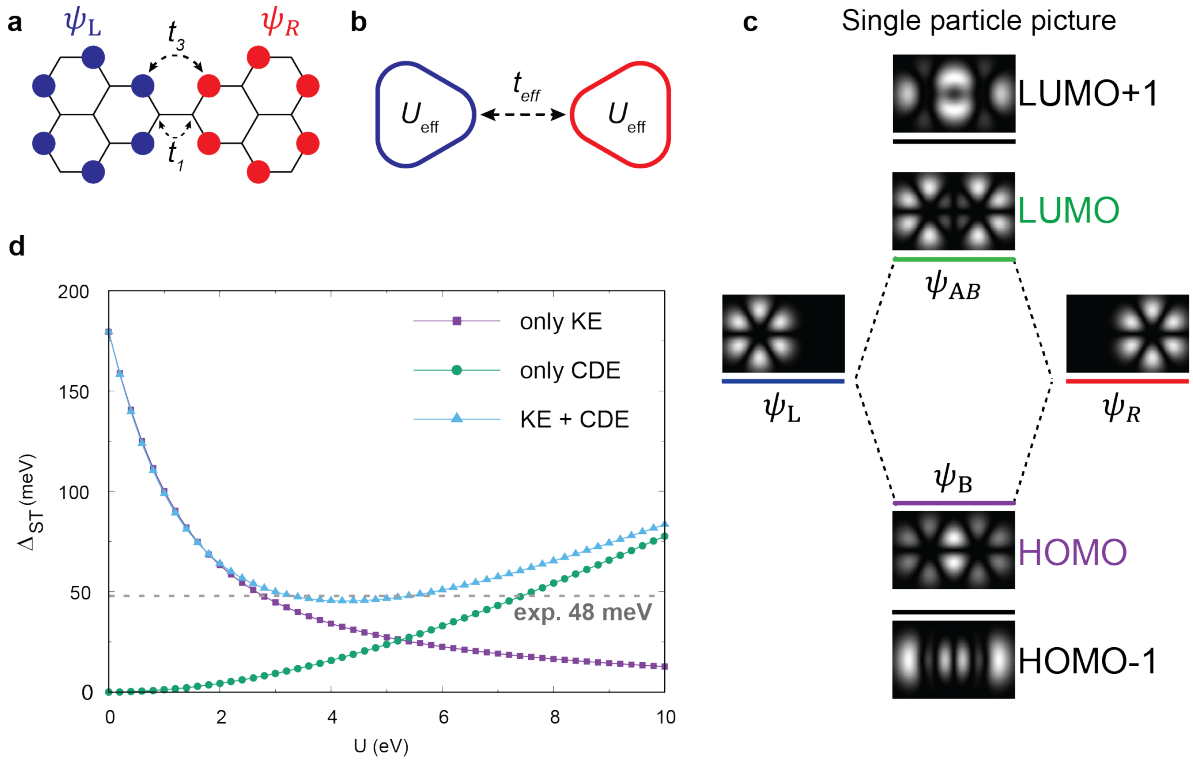

Figure 3. Calculations for extended Hubbard model of diphenalenyl (see SI and Ref. [20]for details). (**a**) Zero mode distribution of diphenalenyl. Due to missing weight at the binding site, the intermolecular hybridization between the two phenalenyl units is driven by third-neighbor hopping t_3 instead of t_1. (**b**) Simplified two-site model of diphenalenyl with effective hopping parameter t_{eff} and effective Coulomb repulsion U_{eff}. (**c**) Molecular orbitals in the single-particle picture. Hybridization of the SOMOs (blue, red) leads to bonding (HOMO, purple) and anti-bonding (LUMO, green) frontier orbitals. (**d**) Singlet–triplet splitting of diphenalenyl as function of Coulomb repulsion for kinetic exchange only (KE, purple squares) and Coulomb driven exchange (CDE, green circles). Considering both exchanges (light blue triangles) predicts a splitting close to the experimentally observed energies (horizontal dashed line) for a wide range of values for the Coulomb repulsion.

There are two mechanisms for intermolecular exchange in this type of system, as discussed by two of us recently.[20] One is driven by intermolecular hybridization of the zero modes of the phenalenyls, the other by Coulomb-mediated virtual occupation of higher-energy extended molecular orbitals. Based on a model with first-neighbor hopping only, one could

expect that intermolecular hybridization vanishes, as the zero-modes have a null weight on the binding sites (as depicted in Figure 3a). Our DFT calculations show that this description is not complete and that hybridization does not vanish (see the SI). This automatically suggests that third-neighbor hopping is non-zero (see figure 3a and also ref.[15]). Therefore, intermolecular hybridization is present, so that the two mechanisms for intermolecular exchange are active and can be accounted for by means of exact diagonalization of the model in a restricted set of multi-electronic states (see the SI). The predictions of this model for the total exchange, and the relative contribution of the two mechanisms are shown in Figure 3d. They show that, for a wide range of values of the Coulomb interactions, the predicted singlet–triplet excitation energy is close to the experimental value. Importantly, the ratio of intermolecular hybridization and intramolecular addition energies show the dimer has a strong diradical character.

We now address the substrate-dependent energy and linewidth of the excitations. To do so, we include in our Hamiltonian the hybridization of the molecular orbitals (MOs) with the conduction electrons in the substrate. Our ab initio calculations show that this hybridization strongly depends on both substrate and MO. (see the SI and refs.[21,22]). The interacting MOs coupled to the conduction electrons in the substrate constitute a multi-orbital Anderson model that we solve in the one-crossing approximation[23] (OCA).

The key quantity that permits to relate the model calculations to the experimental results are the spectral functions of the electrons in the molecule which are directly connected to the dI/dV in the tunneling regime[24] and include both the many-body interactions and the influence of the substrate. We compute the spectral functions $A_k(\omega)$ projected MOs within OCA, taking into account the MOs shown in Figure 3c, i.e. the HOMO-1, HOMO, LUMO and LUMO+1 (see the SI and ref.[21] for details). The results are shown in Figure 4. The coupling to the substrate has two major effects on the system: on the one hand, it leads to screening of the Coulomb tensor, generally lowering the Hubbard U, and therefore modifying the bare excitation energies. On the other hand, the coupling to the substrate gives rise to finite linewidths of the spectral features and relatedly to Kondo exchange which renormalizes the excitation energies[21,25]. In our calculations, the screening of the Coulomb tensor is taken into account by a screening parameter in our model Hamiltonian (see the SI and ref.[20]). Finite

linewidths and Kondo exchange on the other hand are a consequence of solving the Anderson model (by OCA) which includes the single-particle broadening of the MOs due to coupling to the substrate obtained from realistic DFT calculations of the molecule on both surfaces (see the SI and refs.[21,22]).

Our DFT calculations (see the SI) show that in the presence of the NaCl monolayer, the coupling of the molecule to the substrate is very weak. Therefore, renormalization of the excitation energy by Kondo exchange coupling is negligible, and we can account for the experimentally observed excitation energy of ∼ 48 meV in our model, if we take $U \sim 5.4$ eV (c.f. Figure 3d). In contrast, for the Au(111) surface, DFT calculations show that hybridization with the molecule is appreciable, and thus leads to a substantial renormalization (see Figure 4f and the SI). At the same time, we expect the Coulomb interaction in the molecule to be smaller for Au(111) than for the NaCl monolayer due to screening by the conduction electrons. We find good agreement with the experimental value for Au(111) of ∼ 41 meV for a Coulomb interaction tensor corresponding to a Hubbard-U of 2.5 eV. Therefore, we conclude that the observed energy difference is due to a combination of enhanced substrate-induced renormalization and screening of the interactions when the molecules are deposited on Au(111). As expected from previous work[21], the linewidth of the calculated spin-excitation steps is larger for the molecule on Au(111), in agreement with the experiments. It is important to note, however, that the linewidth is somewhat smaller than the experimental value, which probably reflects the limitations of the OCA method.

Finally, we address the origin of the bias asymmetries, both, the generic one seen for both substrates for spectra taken at the central part of the molecule (blue lines in Figure 2a**,**c), as well as the bias asymmetry observed in the spectra taken at the outer parts of the molecule deposited on Au(111). First, we note that the contribution of the HOMO and the LUMO to the step heights (Figure 4a,d) already results in pronounced and opposite asymmetries for both substrates: the HOMO has a significantly larger step for negative bias than for positive bias, while for the LUMO it is exactly the opposite. This asymmetry is ultimately caused by proximity and height of the ion resonance closest to the step, that is, with the same bias polarity. Additionally, in the case of Au(111) the steps show the characteristic triangular overshoots induced by Kondo exchange with the conduction electrons[21,24–29]. The overshoot

is especially pronounced for the positive-bias step in the LUMO spectral function. The reason is the enhancement of the product of the conduction electron density of states $N(E_F)$ and Kondo exchange J_K, given by Γ_{LUMO}/E_A, due to the proximity of the positive ion resonance and thus low electron-addition energy E_A.

The bias and position dependence of the d*I*/d*V* are related to the LDOS that in our many-body picture relates to orbital-resolved spectral function $A_k(\omega)$ as:

$$\rho(\vec{r};\omega) = \sum_k |\psi_k(\vec{r})|^2 A_k(\omega)$$

where the index *k* labels the MO, and $|\psi_k(\vec{r})|^2$ are the square of the MO wave functions. Figures 4c and 4f show the LDOS computed at three different points over the molecule as indicated by the colors corresponding to the circles of the same color in Figure 4b and 4e, respectively. These show the same bias asymmetries observed in the experiment. First, over the center of the molecule (blue line) the LDOS shows the generic asymmetry common to both substrates where the negative bias step is significantly larger than the positive bias step. The reason is the vanishing of the LUMO wave function at the center of the molecule (c.f. Figure 3c). Therefore, the LDOS is dominated by the HOMO spectral function (purple lines in Figure 4a,d). In contrast, both HOMO and LUMO contribute to the LDOS at the outer parts of the molecule (red and black lines in Figure 4c,f). In the case of the NaCl monolayer, this leads to almost symmetric steps, in agreement with experiment (c.f. Figure 2c). On the other hand, for the gold substrate the dominant height of the positive bias step in the HOMO also leads to a predominance of the positive bias step in the LDOS over the side units with the characteristic Kondo exchange induced overshoot, again in agreement with experiment.

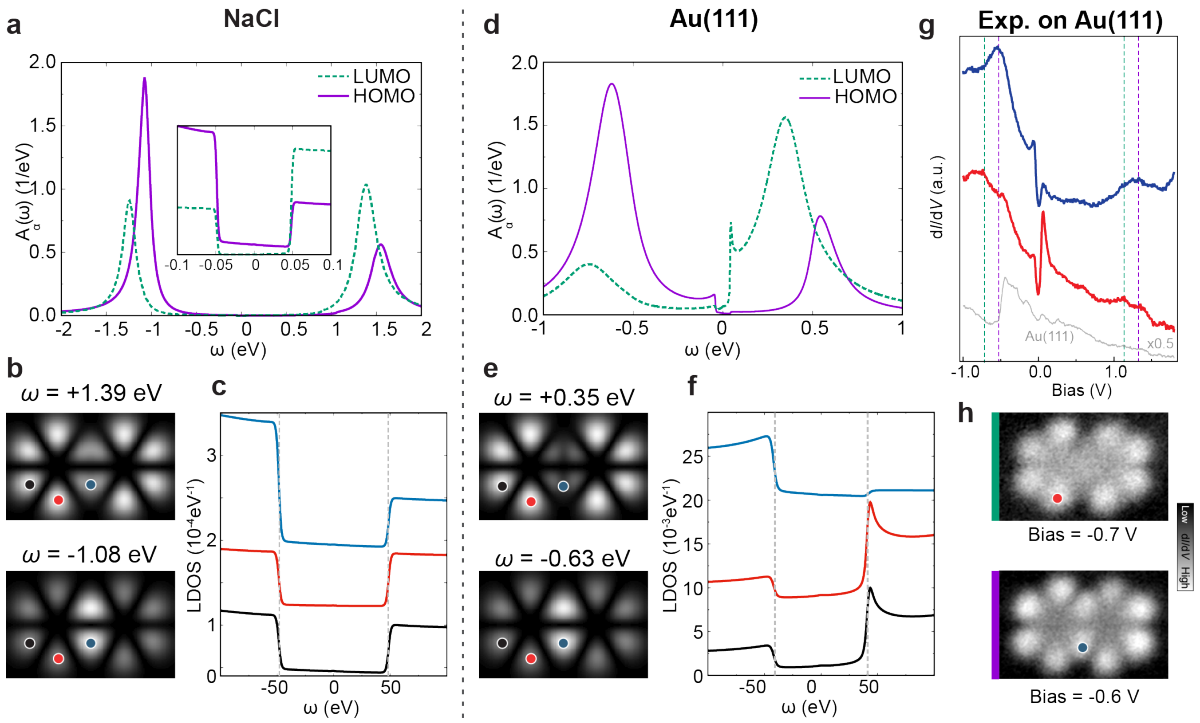

Figure 4. (**a,d**) Spectral function of HOMO (purple) and LUMO (green) for Diphenalenyl on ML-NaCl/Au(111) and Au(111), showing significant spectral weight at both bias polarities. The inset in (a) displays a zoom of the inelastic step features. (**b,e**) Constant height local density of states (LDOS) maps at energies of the highest Hubbard peaks of the HOMO and LUMO spectral functions. (**c,f**) Calculated d*I*/d*V* spectra for different positions, marked by circles in (b,e). Vertical dotted lines mark the singlet–triplet excitation energies. (**g**) Measured d*I*/d*V* spectroscopy taken with CO tip on diphenalenyl on Au(111). The vertical dotted lines indicate the positions of the resonances corresponding to the HOMO (purple) and LUMO (green), for both polarities. Position of spectra are marked by circles in (h). Feedback loop opened at -1 V/350 pA, V_{rms} = 14 mV. (**h**) Measured d*I*/d*V* maps at negative bias voltages, matching the LDOS of the LUMO (top) and HOMO (bottom). Maps taken at 200 pA and V_{rms} = 14 mV.

Figure 4b,e shows LDOS maps, $\rho(\vec{r};\omega)$, computed at the energies ω of the highest Hubbard peak in the HOMO and the LUMO spectral functions for both substrates. These correspond to constant height maps of the d*I*/d*V* at fixed voltage. Clearly, comparison with Figure 3c shows that the LDOS maps at negative energies resemble the density map of the HOMO while those at positive energies resemble the density map of the LUMO. Naturally, the correspondence is not 100% since also the other orbital(s) contribute with some weight.

Further validation of our model, and additional evidence for intermolecular hybridization, comes from the prediction for the molecule on Au(111) of a splitting of the negative ion resonance, that arises from the HOMO–LUMO hybridization splitting, of about 100 meV. In the many-body picture, both MO contribute to the negative ion resonance, at slightly different energies (Figure 4a,b). This prediction is confirmed by STS with a CO-functionalized tip, which, depending on the position of the STM tip over the molecule (shown in the inset), exhibits peaks at different voltages. For the position over one of the lobes at the center of the dimer (blue), where only the HOMO contributes (see Figure 4h, bottom), there is a pronounced peak at around –0.6 V, while at the position away from the center (red), where the LUMO contribution is the strongest (see Figure 4h top), a broader peak around -0.7 V is found. Constant current d*I*/d*V* maps taken at these voltages (Figure 4h, top) further confirm the assignment of these peaks to HOMO and LUMO.

In summary, thorough spectroscopy studies combined with theory portray diphenalenyl as an open-shell molecule, where strong interphenalenyl antiferromagnetic exchange leads to an $S = 0$ ground state and an $S = 1$ excited state. Additionally, we have provided strong evidence for the existence of intermolecular hybridization. The peculiar nature of the zero-modes in this class of system makes it possible to unveil the role of third-neighbor hopping, dominant for these states, and very frequently ignored in the modeling of graphene. By comparing the spectra for the same molecule on two different surfaces, we also show the relevant role of coupling to the substrate, that changes not only the lifetimes, but also the energies of the inelastic excitations. These findings need to be taken into account for the design of platforms that exploit phenalenyl and other planar nanographene radicals as molecular building blocks for quantum technologies such as quantum computing, quantum simulation or quantum sensing.

Associated content

Supporting Information

Experimental and computational methods, supporting STM and STS data, additional calculations, and a detailed synthetic description and characterization of chemical compounds reported in this study (PDF).

Author Contributions

P.R., R.F and M.J conceived the experiments. A.B. synthesized and characterized the precursors in solution. N.K and E.T performed the on-surface synthesis and scanning probe measurements. N.K and E.T performed TB calculations and analyzed the data. D.J, J.F.R and G.G simulated the system using different levels of theory. All authors discussed the results and contributed to the writing of the manuscript.

Funding Sources

This research was supported by the Swiss National Science Foundation (SNSF; Grant No. CRSII5_205987, 200020_18201, PP00P2_170534 and PP00P2_198900), CarboQuant funded by the Werner Siemens Foundation, the EU Horizon 2020 research and innovation program − Marie Skłodowska-Curie grant no. 813036, and ERC Starting grant (INSPIRAL, grant no. 716139). The work was also financially supported from Grant PID2020-112811GB-I00 funded by MCIN/AEI/10.13039/501100011033 and Grant No. IT1453-22 from the Basque Government. The research was also supported by NCCR MARVEL, a National Centre of Competence in Research, funded by the Swiss National Science Foundation (grant number 205602 and by a grant from the Swiss National Supercomputing Centre (CSCS) under project ID s1142. JFR further acknowledges financial support from FCT (Grant No. PTDC/FIS-MAC/2045/2021), Generalitat Valenciana funding Prometeo2021/017 and MFA/2022/045, and MICIIN-Spain (Grant No. PID2019-109539GB-C41).

Acknowledgement

We thank Oliver Gröning, Kristjan Eimre and Carlo Antonio Pignedoli for the fruitful scientific discussions. Skillful technical assistance by Lukas Rotach is gratefully acknowledged.

References

(1) Uchida, K.; Kubo, T. Recent Advances in the Chemistry of Phenalenyl. *J. Synth. Org. Chem. Jpn.* **2016**, *74* (11), 1069–1077. https://doi.org/10.5059/yukigoseikyokaishi.74.1069.

(2) Turco, E.; Bernhardt, A.; Krane, N.; Valenta, L.; Fasel, R.; Juríček, M.; Ruffieux, P. Observation of the Magnetic Ground State of the Two Smallest Triangular

Nanographenes. *JACS Au* **2023**, jacsau.2c00666. https://doi.org/10.1021/jacsau.2c00666.
(3) Hirjibehedin, C. F.; Lutz, C. P.; Heinrich, A. J. Spin Coupling in Engineered Atomic Structures. *Science* **2006**, *312* (5776), 1021. https://doi.org/10.1126/science.1125398.
(4) Mishra, S.; Catarina, G.; Wu, F.; Ortiz, R.; Jacob, D.; Eimre, K.; Ma, J.; Pignedoli, C. A.; Feng, X.; Ruffieux, P.; Fernández-Rossier, J.; Fasel, R. Observation of Fractional Edge Excitations in Nanographene Spin Chains. *Nature* **2021**, *598* (7880), 287–292. https://doi.org/10.1038/s41586-021-03842-3.
(5) Hieulle, J.; Castro, S.; Friedrich, N.; Vegliante, A.; Lara, F. R.; Sanz, S.; Rey, D.; Corso, M.; Frederiksen, T.; Pascual, J. I.; Peña, D. On-Surface Synthesis and Collective Spin Excitations of a Triangulene-Based Nanostar. *Angew. Chem. Int. Ed.* **2021**, *60* (48), 25224–25229. https://doi.org/10.1002/anie.202108301.
(6) Mishra, S.; Beyer, D.; Eimre, K.; Ortiz, R.; Fernández-Rossier, J.; Berger, R.; Gröning, O.; Pignedoli, C. A.; Fasel, R.; Feng, X.; Ruffieux, P. Collective All-Carbon Magnetism in Triangulene Dimers. *Angew. Chem. Int. Ed.* **2020**, *59* (29), 12041–12047. https://doi.org/10.1002/anie.202002687.
(7) Cheng, S.; Xue, Z.; Li, C.; Liu, Y.; Xiang, L.; Ke, Y.; Yan, K.; Wang, S.; Yu, P. On-Surface Synthesis of Triangulene Trimers via Dehydration Reaction. *Nat. Commun.* **2022**, *13* (1), 1705. https://doi.org/10.1038/s41467-022-29371-9.
(8) Pavliček, N.; Mistry, A.; Majzik, Z.; Moll, N.; Meyer, G.; Fox, D. J.; Gross, L. Synthesis and Characterization of Triangulene. *Nat. Nanotechnol.* **2017**, *12* (4), 308–311. https://doi.org/10.1038/nnano.2016.305.
(9) Li, J.; Sanz, S.; Castro-Esteban, J.; Vilas-Varela, M.; Friedrich, N.; Frederiksen, T.; Peña, D.; Pascual, J. I. Uncovering the Triplet Ground State of Triangular Graphene Nanoflakes Engineered with Atomic Precision on a Metal Surface. *Phys. Rev. Lett.* **2020**, *124* (17), 177201. https://doi.org/10.1103/PhysRevLett.124.177201.
(10) Mishra, S.; Beyer, D.; Eimre, K.; Kezilebieke, S.; Berger, R.; Gröning, O.; Pignedoli, C. A.; Müllen, K.; Liljeroth, P.; Ruffieux, P.; Feng, X.; Fasel, R. Topological Frustration Induces Unconventional Magnetism in a Nanographene. *Nat. Nanotechnol.* **2020**, *15* (1), 22–28. https://doi.org/10.1038/s41565-019-0577-9.
(11) Turco, E.; Mishra, S.; Melidonie, J.; Eimre, K.; Obermann, S.; Pignedoli, C. A.; Fasel, R.; Feng, X.; Ruffieux, P. On-Surface Synthesis and Characterization of Super-Nonazethrene. *J. Phys. Chem. Lett.* **2021**, *12* (34), 8314–8319. https://doi.org/10.1021/acs.jpclett.1c02381.
(12) Biswas, K.; Urgel, J. I.; Ajayakumar, M. R.; Ma, J.; Sánchez-Grande, A.; Edalatmanesh, S.; Lauwaet, K.; Mutombo, P.; Gallego, J. M.; Miranda, R.; Jelínek, P.; Feng, X.; Écija, D. Synthesis and Characterization of Peri-Heptacene on a Metallic Surface. *Angew. Chem.* **2022**, *134* (23), e202114983. https://doi.org/10.1002/ange.202114983.
(13) de Oteyza, D. G.; Frederiksen, T. Carbon-Based Nanostructures as a Versatile Platform for Tunable π-Magnetism. *J Phys* **2022**, 42.
(14) Mishra, S.; Yao, X.; Chen, Q.; Eimre, K.; Gröning, O.; Ortiz, R.; Di Giovannantonio, M.; Sancho-García, J. C.; Fernández-Rossier, J.; Pignedoli, C. A.; Müllen, K.; Ruffieux, P.; Narita, A.; Fasel, R. Large Magnetic Exchange Coupling in Rhombus-Shaped Nanographenes with Zigzag Periphery. *Nat. Chem.* **2021**. https://doi.org/10.1038/s41557-021-00678-2.

(15) Ortiz, R.; Catarina, G.; Fernández-Rossier, J. Theory of Triangulene Two-Dimensional Crystals. *2D Mater.* **2022**, *10* (1), 015015. https://doi.org/10.1088/2053-1583/aca4e2.
(16) Repp, J.; Meyer, G.; Paavilainen, S.; Olsson, F. E.; Persson, M. Imaging Bond Formation Between a Gold Atom and Pentacene on an Insulating Surface. *Science* **2006**, *312* (5777), 1196–1199. https://doi.org/10.1126/science.1126073.
(17) Ovchinnikov, A. A. Multiplicity of the Ground State of Large Alternant Organic Molecules with Conjugated Bonds. *Theor. Chim. Acta* **1978**, *47* (4), 297–304. https://doi.org/10.1007/BF00549259.
(18) Lieb, E. H. Two Theorems on the Hubbard Model. *Phys. Rev. Lett.* **1989**, *62* (10), 1201–1204. https://doi.org/10.1103/PhysRevLett.62.1201.
(19) Reecht, G.; Heinrich, B. W.; Bulou, H.; Scheurer, F.; Limot, L.; Schull, G. Imaging Isodensity Contours of Molecular States with STM. *New J. Phys.* **2017**, *19* (11), 113033. https://doi.org/10.1088/1367-2630/aa969a.
(20) Jacob, D.; Fernández-Rossier, J. Theory of Intermolecular Exchange in Coupled Spin- 1 2 Nanographenes. *Phys. Rev. B* **2022**, *106* (20), 205405. https://doi.org/10.1103/PhysRevB.106.205405.
(21) Jacob, D.; Ortiz, R.; Fernández-Rossier, J. Renormalization of Spin Excitations and Kondo Effect in Open-Shell Nanographenes. *Phys. Rev. B* **2021**, *104* (7), 075404. https://doi.org/10.1103/PhysRevB.104.075404.
(22) Gandus, G.; Passerone, D.; Stadler, R.; Luisier, M.; Valli, A. Strongly Correlated Physics in Organic Open-Shell Quantum Systems. arXiv December 31, 2022. https://doi.org/10.48550/arXiv.2301.00282.
(23) Haule, K.; Kirchner, S.; Kroha, J.; Wölfle, P. Anderson Impurity Model at Finite Coulomb Interaction U: Generalized Noncrossing Approximation. *Phys. Rev. B* **2001**, *64* (15), 155111. https://doi.org/10.1103/PhysRevB.64.155111.
(24) Jacob, D. Simulation of Inelastic Spin Flip Excitations and Kondo Effect in STM Spectroscopy of Magnetic Molecules on Metal Substrates. *J. Phys. Condens. Matter* **2018**, *30* (35), 354003. https://doi.org/10.1088/1361-648X/aad523.
(25) Oberg, J. C.; Calvo, M. R.; Delgado, F.; Moro-Lagares, M.; Serrate, D.; Jacob, D.; Fernández-Rossier, J.; Hirjibehedin, C. F. Control of Single-Spin Magnetic Anisotropy by Exchange Coupling. *Nat. Nanotechnol.* **2014**, *9* (1), 64–68. https://doi.org/10.1038/nnano.2013.264.
(26) Žitko, R.; Pruschke, T. Many-Particle Effects in Adsorbed Magnetic Atoms with Easy-Axis Anisotropy: The Case of Fe on the CuN/Cu(100) Surface. *New J. Phys.* **2010**, *12* (6), 063040. https://doi.org/10.1088/1367-2630/12/6/063040.
(27) Korytár, R.; Lorente, N.; Gauyacq, J.-P. Many-Body Effects in Magnetic Inelastic Electron Tunneling Spectroscopy. *Phys. Rev. B* **2012**, *85* (12), 125434. https://doi.org/10.1103/PhysRevB.85.125434.
(28) Ternes, M. Spin Excitations and Correlations in Scanning Tunneling Spectroscopy. *New J. Phys.* **2015**, *17* (6), 063016. https://doi.org/10.1088/1367-2630/17/6/063016.
(29) Jacob, D.; Fernández-Rossier, J. Competition between Quantum Spin Tunneling and Kondo Effect. *Eur. Phys. J. B* **2016**, *89* (10), 210. https://doi.org/10.1140/epjb/e2016-70402-2.
(30) Mugarza, A.; Robles, R.; Krull, C.; Korytár, R.; Lorente, N.; Gambardella, P. Electronic and Magnetic Properties of Molecule-Metal Interfaces: Transition-Metal

Phthalocyanines Adsorbed on Ag(100). *Phys. Rev. B* **2012**, *85* (15), 155437. https://doi.org/10.1103/PhysRevB.85.155437.
(31) Ternes, M.; Heinrich, A. J.; Schneider, W.-D. Spectroscopic Manifestations of the Kondo Effect on Single Adatoms. *J. Phys. Condens. Matter* **2008**, *21* (5), 053001. https://doi.org/10.1088/0953-8984/21/5/053001.

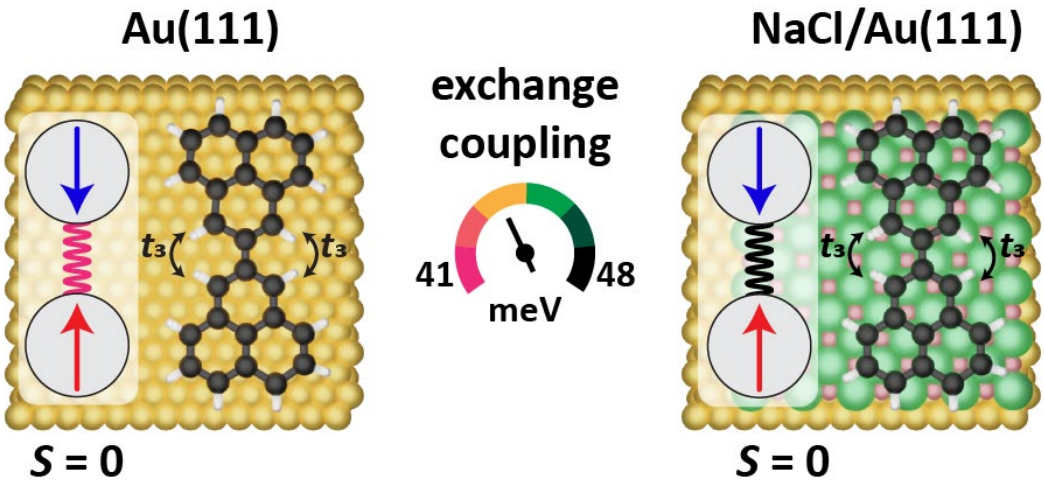

For Table of Contents Only